



# The Evolution of Cracks in Maluanshan Granite Subjected to Different Temperature Processing

Guanghui Jiang<sup>1</sup> · Jianping Zuo<sup>1,2</sup> · Liyun Li<sup>1</sup> · Teng Ma<sup>1</sup> · Xu Wei<sup>1</sup>

Received: 24 July 2017 / Accepted: 4 January 2018 / Published online: 1 February 2018  
© Springer-Verlag GmbH Austria, part of Springer Nature 2018

## Abstract

The understanding of the change in the physical and mechanical properties of rock before and after heating is of great significance for the site selection of mattamore and the exploitation of geothermal resources. It is known that before and after heating, the changes in wave velocity, wave velocity anisotropy and permeability of rock are due to the evolution of cracks in the rock. In this study, the wave velocity and permeability of granite specimen from the Maluanshan tunnel in Shenzhen, China, were measured after high-temperature processing at atmospheric pressure. The effects of temperature on the properties of rock based on the acoustics and permeability were measured and analyzed. The evolution of the cracks in Maluanshan granite was inverted through the change rule of the cracks, wave velocity anisotropy and permeability with temperature. The main conclusions were as follows: (1) Both granite  $P$  and  $S$  wave velocities decreased with the increasing temperature, and the thermal cracking occurred in four stages: between 50 and 250 °C, the crack stabilization development stage was in effect; between 250 and 300 °C, an accelerated development stage of the cracks existed; between 300 and 350 °C, a shift stage for the cracks was entered; and finally, from 350 to 700 °C, the cracks continued into a further development stage; (2) The coefficient of variation could be used to reflect the structural feature change of the rocks in the study of the wave velocity anisotropy. The structures of cracks were observed to change before and after 300 °C. (3) The Maluanshan granite permeability increases with the increasing processing temperature. It was observed that the higher the processing temperature, the larger the increase in the permeability rate. A porosity function was used as a variable to analyze the relationship between the porosity function and permeability as follows: from 50 to 200 °C, the permeability was determined by the microcracks; 200–400 °C was the transition stage; and between 400 and 700 °C, the permeability was determined by the macrocracks.

**Keywords** High temperature · Maluanshan granite · Wave velocity · Coefficient of variation · Permeability

## List of symbols

$A$  Initial sectional area of specimen ( $L^2$ )  
 $B$  Geometrical factor (–)  
 $CV$  Coefficient of variation (–)  
 $d$  Particle size ( $L$ )  
 $k$  Permeability ( $L^2$ )  
 $L$  Initial length of specimen ( $L$ )  
 $N$  Degree of freedom (–)  
 $\Delta P_f$  Final osmotic pressure difference ( $M L^{-1} T^{-2}$ )

$\Delta P_i$  Initial osmotic pressure difference ( $M L^{-1} T^{-2}$ )  
 $SD$  Standard deviation (–)  
 $\Delta t$  Testing time ( $T$ )  
 $T$  Temperature ( $K$ )  
 $T_0$  Normal temperature ( $K$ )  
 $v$  Wave velocity in rock ( $L T^{-1}$ )  
 $v_0$  Wave velocity at normal temperature ( $L T^{-1}$ )  
 $\bar{v}$  Average wave velocity ( $L T^{-1}$ )  
 $v_{fl}$  Wave velocity in pore fluid ( $L T^{-1}$ )  
 $v_i$  Wave velocity of point  $i$  ( $L T^{-1}$ )  
 $v_m$  Wave velocity in matrix ( $L T^{-1}$ )  
 $V$  Volume of pressure vessel ( $L^3$ )  
 $\beta$  Coefficient of volume compressibility (–)  
 $\mu$  Coefficient of kinetic viscosity ( $M L^{-1} T^{-1}$ )  
 $\rho$  The density of rock ( $M L^{-3}$ )  
 $\rho_{fl}$  The density of pore fluid ( $M L^{-3}$ )  
 $\rho_m$  The density of matrix ( $M L^{-3}$ )  
 $\varphi$  The porosity of rock (–)

✉ Jianping Zuo  
zjp@cumtb.edu.cn

<sup>1</sup> School of Mechanics and Civil Engineering, China University of Mining and Technology, Beijing 100083, China

<sup>2</sup> State Key Laboratory of Coal Resources and Safe Mining, China University of Mining and Technology, Beijing 100083, China

- $\varphi_0$  Initial porosity at normal temperature (–)  
 $\Delta\varphi$  Porosity difference value (–)

## 1 Introduction

In recent years, with the continuous demand on resources, the depths of mining are increasing, and the influence of temperature on rock has become more prominent. In such projects as mattamore to store nuclear waste, high-temperature reservoir stratum, geothermal fields and flame drilling, it has become paramount to take the effect of high temperature into consideration. Also, it is of great importance for the site selection of mattamore and exploitation of geothermal resources to study the changes in the physical and mechanical property of rock prior to and following heating.

It is known that the changes in wave velocity, wave velocity anisotropy and permeability are the evolution process of cracks in rock prior to and after heating. Simmons and Cooper (1978) and Richter and Simmons (1974) considered that the thermal cracks in rock were related to thermal stress caused by the different thermal expansivity among various rock compositions. Lin (2002) proposed that the thermal cracks in granite are caused by the explosion of fluid inclusion under high temperatures.

Many previous research studies have examined the changes in the physical and mechanical properties of rock with heat treatment. From the aspect of the acoustic properties, after monitoring granite acoustic emissions during heating processes, Xi (1994) and Jones et al. (1997) found that there were two peak values of the acoustic emission rate. These two peak values were determined to correspond to the threshold temperature of the acoustic emission and the phase transition temperature of the quartz, respectively. Nara and Kaneko (2007) utilized *P* wave velocities to analyze the propagation rules of cracks in granite under different temperatures and humidity. It was determined from the results of their study that the propagation of cracks caused by stress corrosion could be effectively monitored by the *P* wave velocity. Inserra et al. (2013) studied the influence of thermal damage on the linear and nonlinear acoustic properties of granite.

From the aspect of permeability, Weinbrandt et al. (1975) studied the effects of temperature on the permeability of sandstones. They were able to determine that thermal stress caused the expansion of rock particles. However, it was found that the interfacial force between the rocks and fluids did not change the absolute permeability of the rock. Unlike Weinbrandt's study, Casse and Ramey (1979) found that the effects of temperature on the permeability of agglutinating sandstones were connected with the properties of the saturated fluid. Morrow et al. (1981) measured the changes in the permeability of

granite as water flowed through samples in a temperature gradient. Jones et al. (1997) observed that the permeability remained constant up to 300 °C. However, above 300 °C, there was a rapid increase in permeability. In the study conducted by Chen et al. (1999), it was believed that the thermally induced fracturing appeared in the boundaries of the rock mineral grains due to the different thermal expansions of the various minerals within the rock during the heating process. It was observed that when the microscopic fracturing was connected similar to a network, the macroscopic permeability and fluid transport properties of the rock changed remarkably. Benson et al. (2006a, b) modeled the permeability evolution of microcracked rocks with different void space geometries at elevated pressures. The relationship between wave velocity and permeability was attempted to be established in their study. Takarli and Prince-Agbodjan (2008) measured the open porosity, gas permeability, *P* wave velocity and their attenuation, ultimate strength, and Young's modulus in samples heated at temperatures ranging from 105 to 600 °C. Chaki et al. (2008) and Chen et al. (2017) studied the influence of thermal damage on the physical properties of granite, and their results revealed similar findings. For example, from 105 to 300 °C, the permeability was observed to increase slightly. Then, between 300 and 500 °C the permeability markedly increased and finally increased by 2–3 orders of magnitude when the temperature exceeded 500 °C. Zhang et al. (2016) found that, in the range of 200–300 °C, the loss of the strong bound water led to an increased number of microcracks, and a better connectivity.

From a microscopic aspect, Homand-Etienne and Houpert (1989) conducted an intensive study of thermal cracks in compact granite. Their results revealed that after heat treatments, the permeability of the rock had increased, and some new cracks had appeared. The lengths of the new cracks were dependent on the grain shapes and sizes. Zuo et al. (2007, 2011) utilized SEM to study the thermal cracking of sandstone and Beishan granite under different temperatures. Chen et al. (2008) used a fluorescent approach to research the microcosmic structure of Westerly granite and Fujioka granite subjected to high-temperature treatments and summarized the crack development at various temperatures. Freire-Lista et al. (2016) exposed four types of granite to forty-two thermal cycles and found that the microcracking which was generated in the granite had barely any impact on their petrophysical properties. Then, using petrographic and fluorescence microscopy, they determined that pre-existing microcracks have coalesced and generated further microcracking as the decay progressed. Freire-Lista and Fort (2017) also selected Alpedrete granite to study the anisotropy of petrophysical properties, such as ultrasonic wave propagation, capillarity, air permeability, microroughness and surface hardness.

Despite the large amount of studies which have been previously conducted, few had correlated multiple factors in order to explain the evolution of cracks in rock undergoing temperature treatments. Therefore, this study focused its attention on granite in order to measure its wave velocity, wave velocity anisotropy and permeability following high-temperature processing at atmospheric pressure, and to obtain the change of rock with temperature.

## 2 Experiments

### 2.1 Specimens

The rock used in this study's experiment was granite from the Maluanshan tunnel in Shenzhen, China. The landform of the Maluanshan tunnel was a hilly topography, with severe undulation. The rock used in the experiment was from the advanced exploration PY2-SD-36, which was located in the right line of the Maluanshan tunnel between YK4 + 360 and YK4 + 380, near the Anshan-Tiantoushan fault zone. The Maluanshan granite is the Yanshanian biotite coarse-grained granite. The specimens were all from a slightly weathered

zone at a depth of 150 m. The cracks in this lightly weathered zone were only slightly developed, and the majority were closed. The core recovery of the drilling hole located in this zone was approximately between 75 and 100%. The mean value of the RQD (Rock Quality Designation) was determined to be 77%. The engineering geological map of Maluanshan tunnel is shown in Fig. 1. The specimens used in this study's experiment are shown in Fig. 2. The basic parameters of the granite specimens are shown in Table 1.



Fig. 2 Core specimens

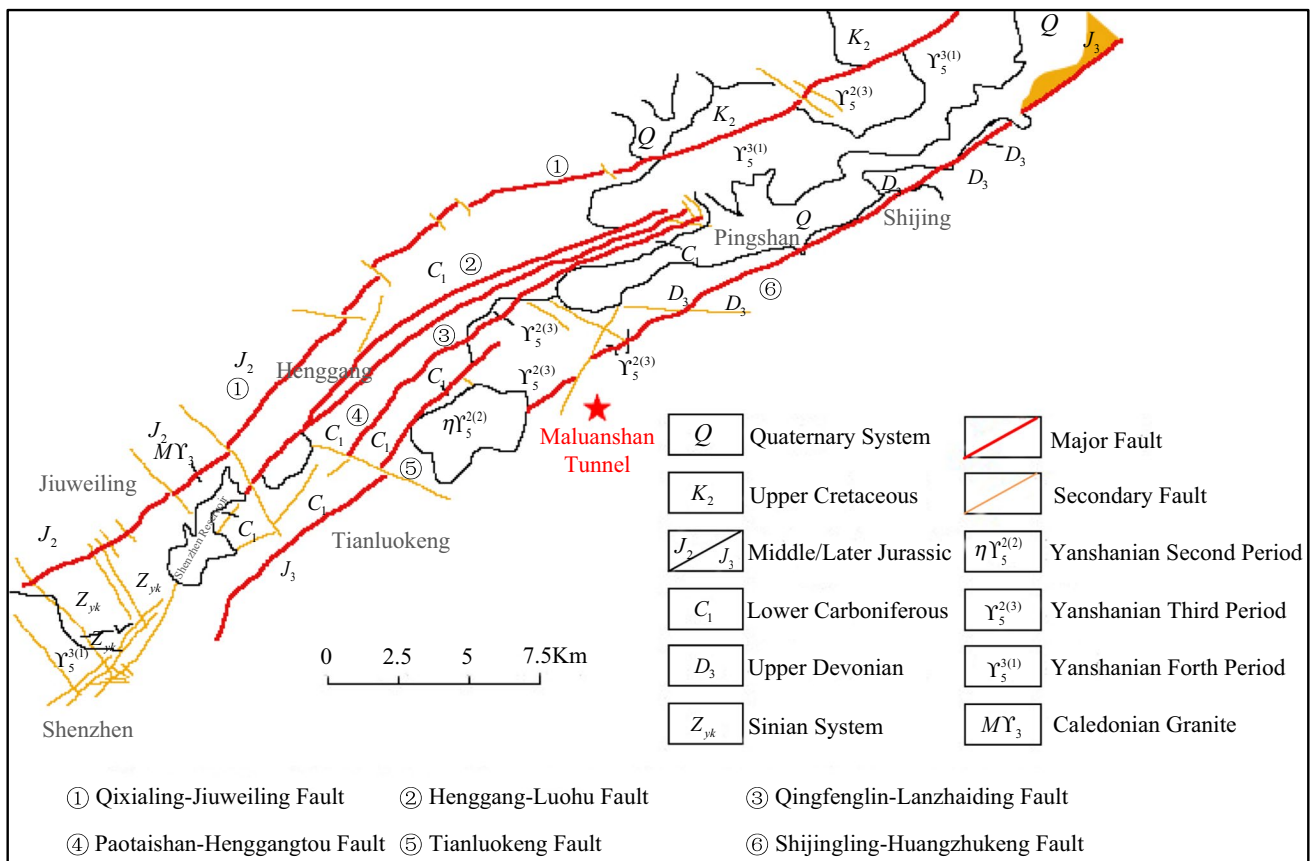


Fig. 1 Engineering geological map of the Maluanshan tunnel

**Table 1** Basic parameters of the granite specimens

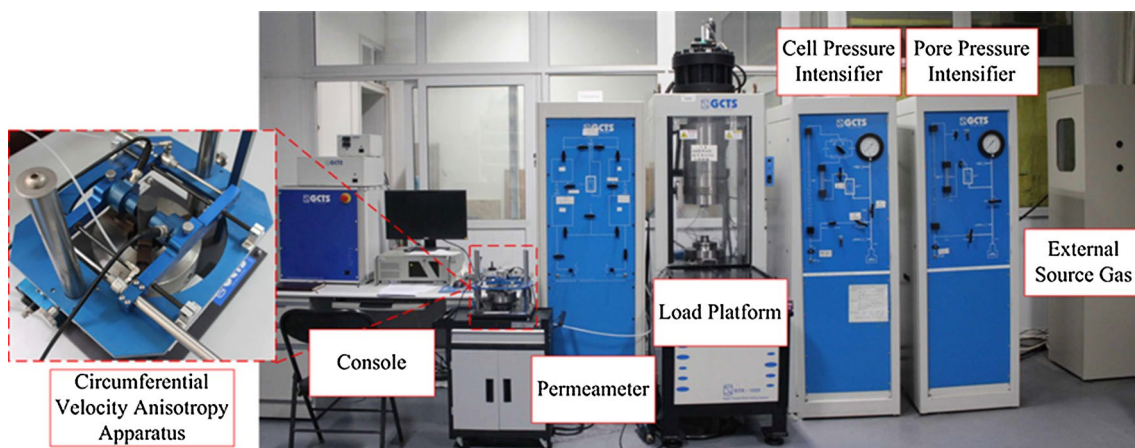
Specimen number	Size		Mass (g)	Density (g/cm <sup>3</sup> )
	Height (mm)	Diameter (mm)		
1	99.92	50	509.84	2.60
2	100.25	50.11	511.40	2.59
3	100.14	50.01	510.91	2.60

## 2.2 Testing Equipment

This study utilized an RTR-1000 rapid triaxial rock testing system obtained from the Geotechnical Consulting and Testing Systems (LLC) to measure the wave velocity and permeability of the samples, as shown in Fig. 3. The testing system included a console, load platform, cell pressure intensifier, pore pressure intensifier, permeameter, external source gas and a circumferential velocity anisotropy apparatus (CVA). Also, a SX<sub>2</sub>-12-12A box-type high-temperature stove was used to heat the specimens. The heating rate of the stove ranged up to 10 °C/min, and the accuracy of steady temperature control was ≤ 1 °C.

## 2.3 Testing Procedures

1. *Drying of Specimens* Since the granite permeability which was measured in the experiment was found to be very low, N<sub>2</sub> was adopted as the permeability media. Therefore, the specimens needed to be dried prior to measurement of the permeability at normal temperature. Thermal cracking was found to occur at temperatures between 60 and 70 °C for the Westerly granite; 70 °C for the Barre granite; and 75 °C for the Charcoal granite (Yong and Wang 1980; Richter and Simmon 1974; Bauer and Johnson 1979). Therefore, in order to avoid
2. *Permeability Measurement* A pulse decay method was used to measure the permeability in this study's experiment. N<sub>2</sub> was injected to saturate the specimens under the conditions of an axial stress of 0.5 MPa, and a confining pressure 5 MPa. Then, pore pressure was applied on one side of the specimen, which remained unchanged while the other side was reduced. The permeability under these conditions could be obtained from the osmotic pressure difference between the two sides over the testing time using Eq. (1) as follows:
 
$$k = \mu\beta V \left( \frac{\ln \left( \frac{\Delta P_i}{\Delta P_f} \right)}{2\Delta t \frac{A}{L}} \right) \quad (1)$$
 where  $\mu$  is the coefficient of the kinetic viscosity, Pa s;  $\beta$  is the coefficient of the volume compressibility, Pa<sup>-1</sup>;  $V$  is the volume of pressure, m<sup>3</sup>;  $\Delta P_i$  is the initial osmotic pressure difference, Pa;  $\Delta P_f$  is the final osmotic pressure difference, Pa;  $\Delta t$  is the testing time, s;  $A$  is the initial sectional area of specimen, m<sup>2</sup>; and  $L$  is the initial length of the specimen, m.
3. *Wave Velocity Anisotropy Measurement* The wave velocities of Specimens P and S were measured using CVA. Honey was used as a coupling agent. Then, from 0 to 170°, the wave velocities were measured every other 10°. The wave velocities at every angle were taken the average of five measurements.
4. *High-Temperature Processing* Following the completion of the wave velocity anisotropy measurement, the specimens were processed in a high-temperature oven.

**Fig. 3** RTR-1000 rapid rock triaxial testing system

The heating rate was maintained at 2 °C/min. When the temperature reached 100 °C, the specimens were maintained at a uniform temperature for three hours and then naturally cooled to a normal temperature in the oven. All heat treatments are at atmospheric pressure.

5. Steps (2) (3) (4) were repeated, with the heat treatment temperatures successively reaching the following: 50, 200, 250, 300, 350, 400, 450, 500, 550, 600, 650 and 700 °C.

The wave velocity, wave velocity anisotropy and permeability of each of the specimens were measured following the different heat treatment temperatures.

### 3 Experimental Results and Analysis

#### 3.1 Change of the Wave Velocity with Temperature

It is known that when wave transmits in rock through grains and cracks, its velocity within the grains is higher than that within cracks. With increasing temperatures, the wave velocity tends to decrease due to the increases number and sizes of cracks which affects the travel path. Therefore, changes in the wave velocities can be indicators of the crack development in rock. Figure 4 shows that the wave velocity decreased with the increasing temperatures.

The wave velocity was found to drop significantly at 300 and 650 °C, which indicated that there were large numbers of cracks produced and developed at these two temperatures. When the cracks were produced and expended in the rock, energy was released in the form of acoustic emissions. Jones et al. (1997) conducted acoustic emission tests with Ailsa Craig microgranite from Scotland and observed that there were two acoustic emission rate peak values during the

heating process, which occurred at 335 °C, and at between 610 and 650 °C, with high energy releases. In this study, the wave velocity swoops at 300 and 650 °C were believed to also correspond with two similar acoustic emission rate peak values.

When compared with the wave velocity at 300 °C, the wave velocity at 350 °C showed only slight changes, along with a possible reverse trend. This confirmed that the number of cracks had only minimally changed from 300 to 350 °C. Fredrich and Wong (1986) counted the number of cracks in Westerly granite following high-temperature processing. The results showed that the number of cracks has increased with the increasing temperatures. It was observed that the number of cracks increased quickly at between 100 and 165 °C and then decreased between 165 and 200 °C, as shown in Fig. 5. Zuo et al. (2011) found similar results in their study of Beishan granite. The experimental results indicated that some of the cracks had a tendency to close after 250 °C, as shown in Fig. 6. Since the closing trend temperature was far lower than the fusion point of various compositions in the granite, partial melting was observed to appear around the plagioclase, microcline and quartz grains at 1000 and 1050 °C (Dang et al. 2016). It was determined that the closures of the cracks were not caused by the hot melting. Zhao et al. (2012) used a self-developed high-temperature and high-pressure triaxial compression system to study the properties of rock. They were able to obtain the linear thermal expansion coefficient of granite under different temperatures, with a downward tendency observed between 200 and 250 °C. These findings corresponded well with the crack closure phenomenon.

It is known that different granite components have different thermal expansivities. When rock is heated, some stress concentration areas will occur. Also, the original cracks will become more developed due to the stress concentrations.

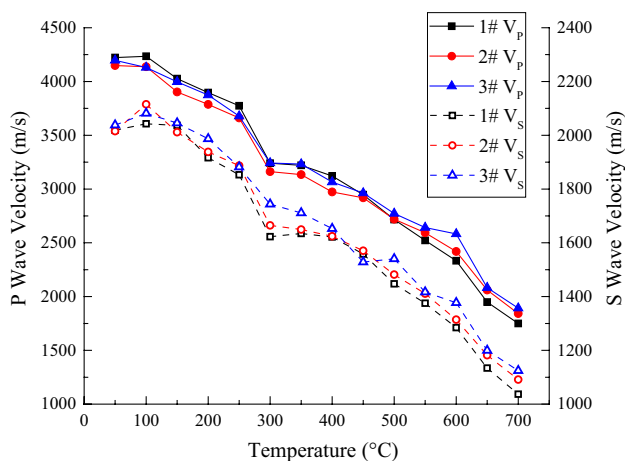


Fig. 4 Change of the average wave velocity with temperature

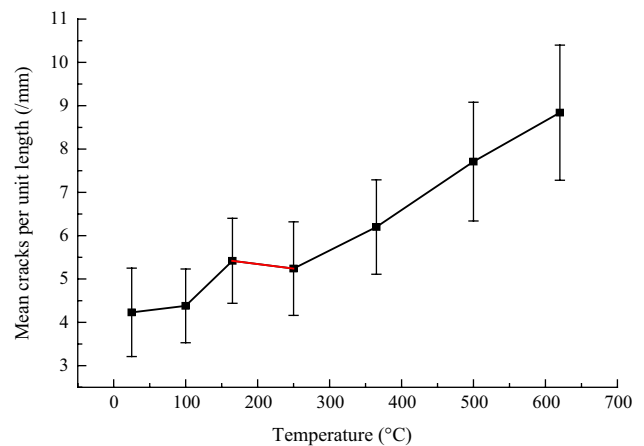
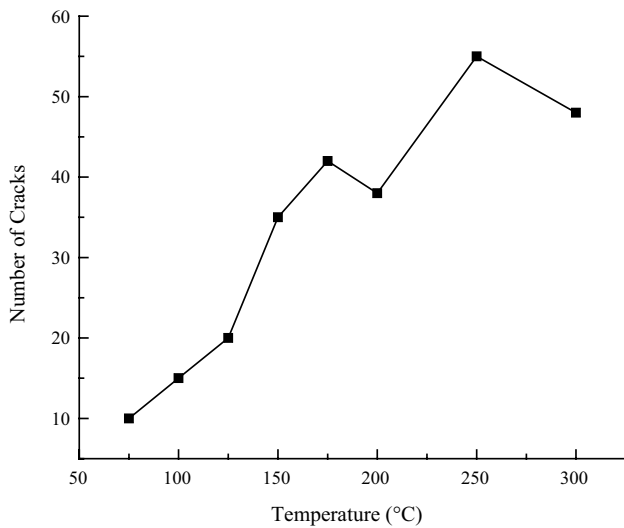


Fig. 5 Number statistics of the thermal cracks in Westerly granite (Fredrich and Wong 1986)



**Fig. 6** Number statistics of the thermal cracks in Beishan granite (Zuo et al. 2011)

With the increase in temperature, some new cracks will occur. In this study, the microcracks included intragranular cracks, intergranular cracks occurring astride the grains on both sides and grain boundary cracks which were formed

along the grain boundaries (Lin 2002). This study analyzed the thermal cracking in four stages, as shown in Fig. 7. By taking #1 as an example, a corresponding stage analysis of the average wave velocity was completed, as shown in Fig. 8.

**Stage I: Microcrack Stabilization Development Stage** During this stage, when the rock was taken from underground of a depth of 150 m, the rock underwent a crustal stress relief, forming a large number of microcracks. The direction of the microcracks correlated with the direction of the crustal stress. Also, the microcracks were observed to be predominantly distributed in the direction perpendicular to the maximum principal stress.

**Stage II: Microcrack Accelerated Development Stage** During this stage, with the increasing temperatures, stress concentration areas and thermal stress increased. The microcracks appeared and extended rapidly, resulting in the dimensions (length, width and aperture) of the microcracks becoming increased.

**Stage III: Crack Shift Stage** When the densities of the microcracks reached a certain value, some of the microcracks combined to form large-sized penetrating cracks during the crack shift stage. The thermal stress was redistributed, which resulted in the closure of some of the microcracks. The formation of some macrocracks and the closure

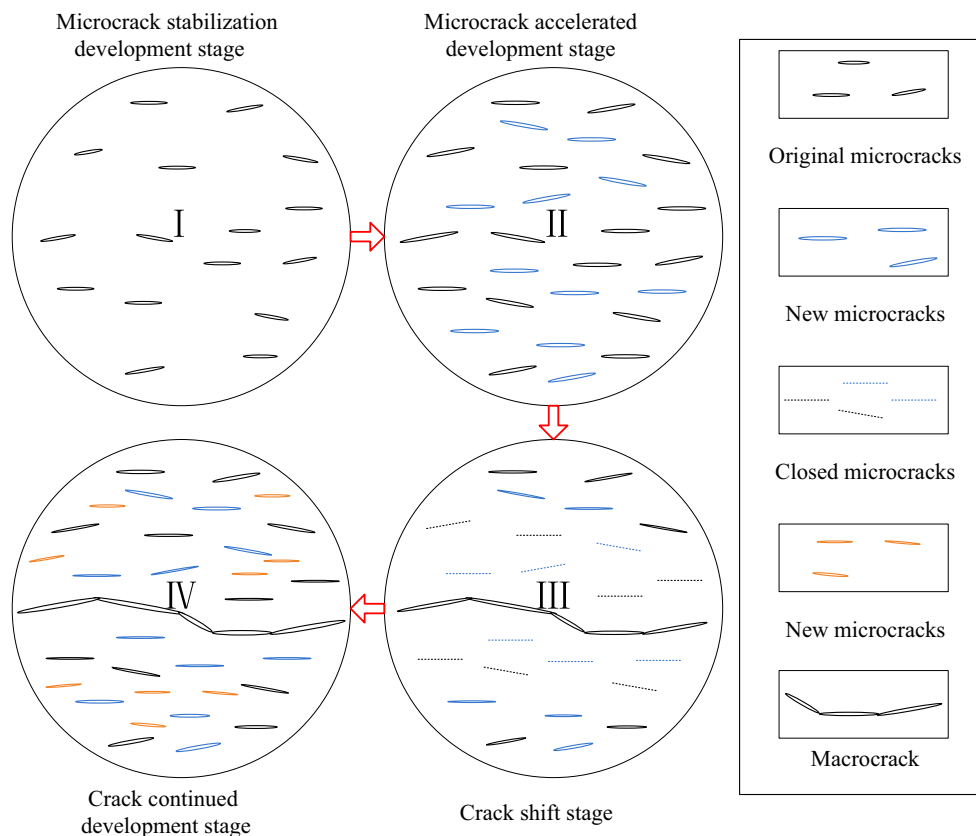


**Fig. 7** Schematic representation of the crack development during the thermal cracking process

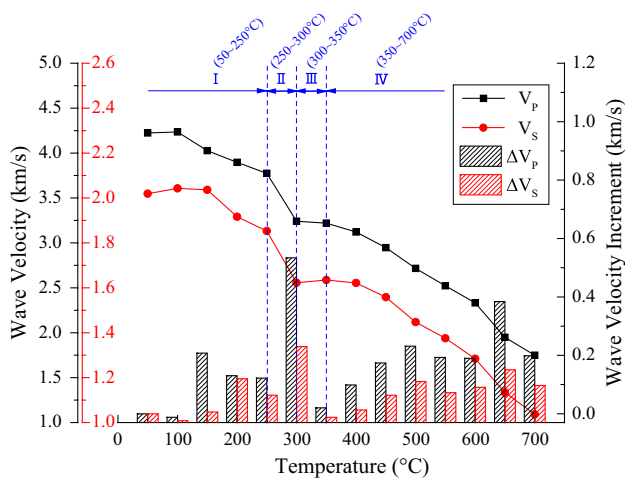


**Fig. 8** #1 change rule and stage analysis of the average wave velocity with temperature

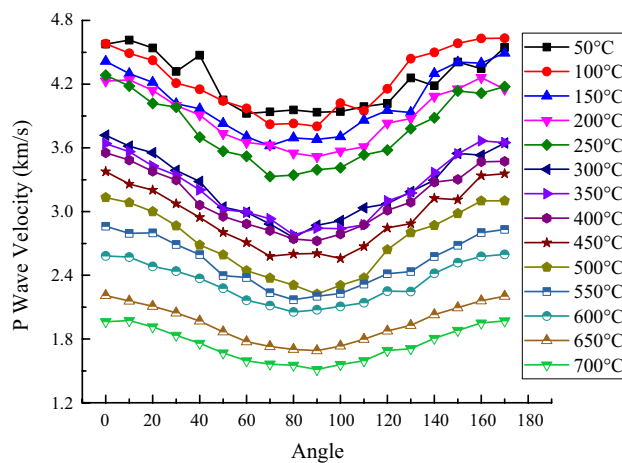
of some microcracks formed an equilibrium state, and the wave velocity remained at a constant value.

Stage IV: *Crack Continued Development Stage* During the fourth stage, with the continued increasing temperatures, the thermal stress further increased, which resulted in a continuous development of the cracks and a decrease in the wave velocity.

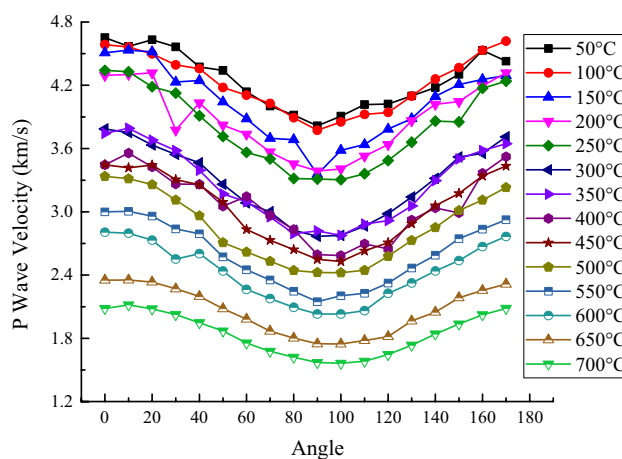
### 3.2 Change of the Wave Velocity Anisotropy with Temperature

In this study, after each of the heat treatments, the wave velocity anisotropy of the rock specimen was measured at the same position. The results are shown in Fig. 9. As can be seen in the figure, the wave velocities at every angle decreased with the increasing temperatures, and with marked changes in the wave velocity observed at between 250 and 300 °C, and between 600 and 650 °C. As mentioned earlier, the microcracks which were produced by the crustal stress relief were predominantly distributed in the direction perpendicular to the maximum principal stress. Therefore, the wave velocity anisotropy could pinpoint the direction of the crustal stress, and the direction of the lowest wave velocity was found to be in the direction of the maximum principal stress. As detailed in Fig. 10, the directions of the wave velocity anisotropy remained unchanged following the heating treatment at different temperatures, which indicated the directionality of the thermal cracks. The propagating directions of the original cracks, and the checking directions of the new cracks, all correlated with the direction of the crustal stress and were perpendicular to the direction of the maximum principal stress, as illustrated in Fig. 8.

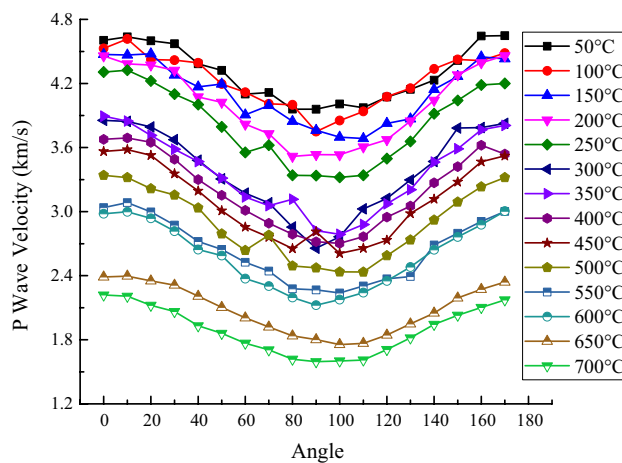
There are many parameters used to reflect the anisotropy, such as the amplitude (difference between the maximum and



**(a) #1**



**(b) #2**



**(c) #3**

**Fig. 9** Change of the wave velocity anisotropy with temperature

minimum wave velocities); ratio of the amplitude and the wave velocity mean value, standard deviation and coefficient of variation. In this study, the coefficient of variation was

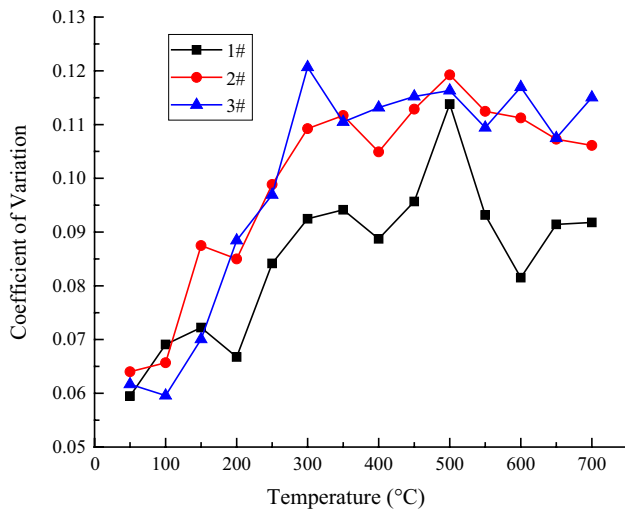


Fig. 10 Change of the coefficient of variation with temperature

chosen to reflect the hoop wave velocity anisotropy. The coefficient of variation can reflect the data dispersion degree, and the value is not only affected by the data dispersion degree, but also affected by the data mean. The coefficient of variation can also eliminate the effects of the units and data mean on the variation degree. Since the wave velocities at different depth are different, the coefficient of variation can be used to reflect the anisotropy. The computational formula of the coefficient of variation (CV) was as follows:

$$CV = (SD/\bar{v}) \times 100\% = \frac{\sqrt{\frac{1}{N} \sum_{i=1}^N (v_i - \bar{v})^2}}{\bar{v}} \times 100\% \quad (2)$$

where SD is the standard deviation;  $N = n - 1$  denotes the degree of freedom;  $v_i$  represents the wave velocity of point  $i$ , m/s; and  $\bar{v}$  is the average wave velocity, m/s.

Figure 10 illustrates the change rule of the coefficient of variation with temperature. It can be seen in the figure that the coefficient of variation increased with the increasing temperatures below 300 °C and almost remained unchanged with the temperatures above 300 °C. The effects of the sub-orbicular pore structure on wave velocities in every direction were observed to be the same, and no effects were observed on the coefficient of variation. The differences among the wave velocities in the different directions were mainly caused by the crack structures. It was confirmed that the crack structures were the main influence factors on the coefficient of variation. The coefficient of variable can be used to reveal the crack structural feature changes of rock in studies regarding wave velocity anisotropy. The effects of temperature on the change of the average wave velocity suggested that the structures of the crack underwent changes when the temperatures reached 300 °C. However,

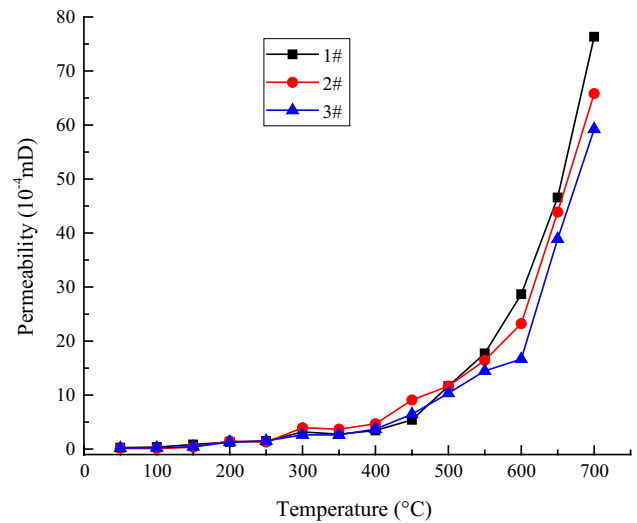


Fig. 11 Change of the permeability with temperature

above 300 °C, the crack changes were mainly observed to be increase in the dimensions (length, width and aperture) of the microcracks. Also, below 300 °C, the changes in cracks were mainly the results of the transformations of the microcracks to macrocracks.

### 3.3 Change of the Permeability with Temperature

It was found in this study that the permeability increased at high temperatures as a result of the development of pores and cracks, as shown in Fig. 11. It was observed that the permeability at 700 °C had increased by several hundred times when compared to that at normal temperature. Figure 12 details the change of the #1 permeability and its variables with temperature. It was observed that there was an obvious downtrend at 350 °C, which corresponded to a slight change in the wave velocity. The other two specimens showed a similar behavior.

Raymer et al. (1980) improved on Wyllie’s equation to obtain the empirical formula of the wave velocity–porosity as follows:

$$\begin{cases} v = (1 - \varphi)^2 v_m + \varphi v_{fl}, & \varphi < 37\% \\ \frac{1}{\rho v^2} = \frac{\varphi}{\rho_{fl} v_{fl}^2} + \frac{1 - \varphi}{\rho_m v_m^2}, & \varphi > 37\% \end{cases} \quad (3)$$

where  $\varphi$  represents the porosity of the rock;  $v$ ,  $v_m$  and  $v_{fl}$  are the wave velocities in the rock, matrix and pore fluid, respectively, m/s; and  $\rho$ ,  $\rho_m$  and  $\rho_{fl}$  denote the rock densities, matrix and pore fluid, respectively, kg/m<sup>3</sup>.

The permeability of granite is known to be very low, and therefore, only the first part of Eq. (3) was needed to calculate the porosity. The equation was further improved with the porosity at normal temperature  $T_0$  measured by a liquid



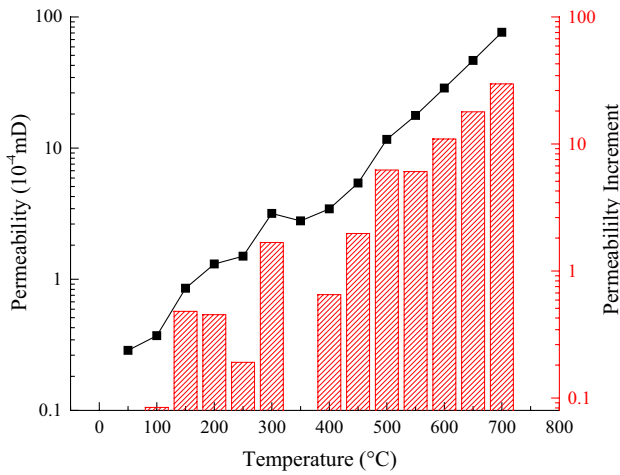


Fig. 12 Change of #1 permeability and its variables with temperature

saturation method as the initial porosity  $\varphi_0$ . Equation (3) was used to calculate the porosity difference  $\Delta\varphi$  between  $\varphi$  at temperature  $T$  and  $\varphi_0$  at normal temperature  $T_0$ :

$$\varphi = \varphi_0 + \Delta\varphi \tag{4}$$

Then, according to Eq. (3):

$$\Delta\varphi = \frac{-m - \sqrt{m^2 + 4v_m\Delta v}}{2v_m} \tag{5}$$

where  $m = -\sqrt{v_{fl}^2 + 4v_m(v_0 - v_{fl})}$ ;  $\Delta v = v - v_0$ ; and  $v_0$  is the wave velocity at normal temperature  $T_0$ , with the unit m/s.

By combining Eqs. (4) and (5), the porosity could be obtained as follows:

$$\varphi = \varphi_0 - \frac{m + \sqrt{m^2 + 4v_m(v - v_0)}}{2v_m} \tag{6}$$

The porosities of the granite at different temperatures were calculated. It was found that porosity increased with the increasing temperatures.

This study’s experimental results showed that during heating processes, the main changes in rock were the changes in the crack structures, which resulted in changes in the permeability and wave velocity. Therefore, it was observed that there was a clear correlation between the permeability and the wave velocity through the porosity. Carman and Machefer (1961) provided a method to estimate the pore medium permeability using the porosity, superficial area and particle sizes as follows:

$$k = Bd^2 \frac{\varphi^3}{(1 - \varphi)^2} \tag{7}$$

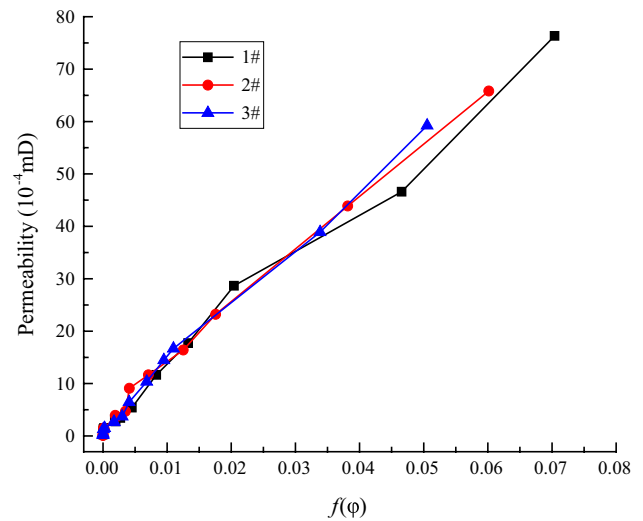


Fig. 13 Change of the permeability with  $f(\varphi)$

where  $B$  is the geometrical factor;  $d$  is the particle size, m; and  $\varphi$  denotes the porosity.

The function  $f(\varphi) = \frac{\varphi^3}{(1-\varphi)^2}$  was used as the variable to analyze the relationship between the porosity function  $f(\varphi)$  and permeability  $k$ , as shown in Fig. 13.

It was determined under close examination that the relationship between the permeability and porosity function was an approximate piecewise linear function. The product of the geometrical factor and particle size varied at different stages. These findings were also related to the crack development. For example, #3 specimen was used to demonstrate the piecewise fit as follows: During *Stage 1* (50–200 °C), a large slope indicated a quick change in permeability with the porosity function, and the permeability was determined by the microcracks; In *Stage 2* (200–400 °C), the small value of the slope showed a slow change in the permeability with the porosity function, and was considered to be a transition stage; a slightly higher slope than that of stage 2 was obtained in *Stage 3* (400–700 °C), and the permeability was determined by the macrocracks. Figure 14 reveals that all of the data fit with the Kozeny–Carman Equation to a high degree at every stage. Table 2 shows the segmentation fitting results of the change rule of permeability with the porosity function. The fitting degrees of all the specimens suggested the segmentation was reasonable.

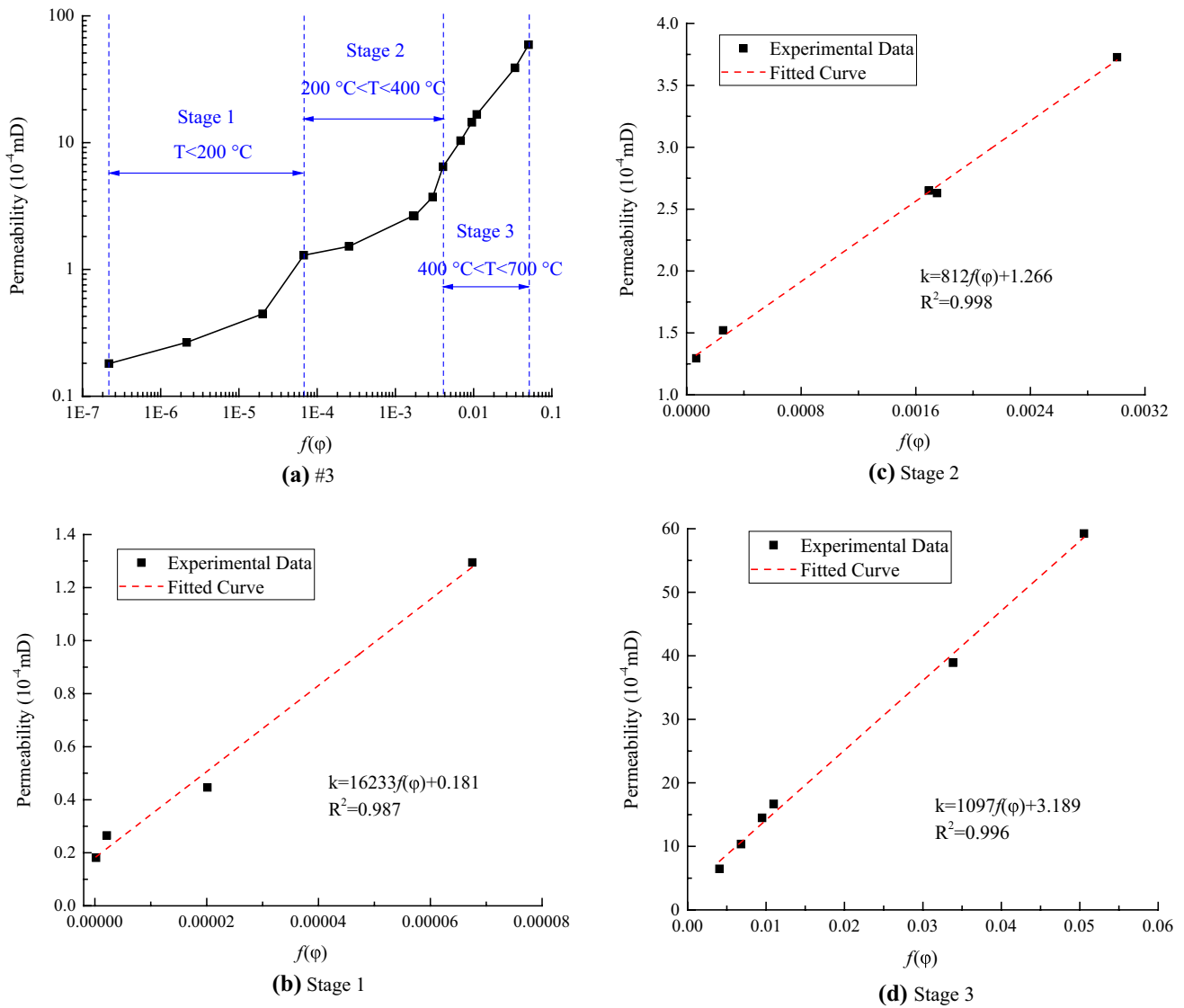


Fig. 14 Segmentation fitting of the change of the permeability with  $f(\varphi)$  of the #3 specimen

Table 2 Segmentation fitting results of the permeability change with  $f(\varphi)$

Stage	Sample	Fitted curve	A	B	R <sup>2</sup>
Stage 1	#1	$k = 13,979f(\varphi) + 0.39638$	13,979	0.396	0.881
	#2	$k = 14,632f(\varphi) + 0.05796$	14,632	0.058	0.940
	#3	$k = 16,233f(\varphi) + 0.18146$	16,233	0.181	0.987
Stage 2	#1	$k = 817f(\varphi) + 1.33911$	817	1.339	0.944
	#2	$k = 1042f(\varphi) + 1.38474$	1042	1.385	0.925
	#3	$k = 812f(\varphi) + 1.26588$	812	1.266	0.998
Stage 3	#1	$k = 1016f(\varphi) + 3.37391$	1016	3.374	0.983
	#2	$k = 1021f(\varphi) + 4.57822$	1021	4.578	0.999
	#3	$k = 1097f(\varphi) + 3.18941$	1097	3.189	0.996

### 4 Inversion of the Cracks with Different Parameters

The change of the wave velocity and coefficient of variation with the temperatures, as well as the wave velocity–permeability model, were piecewise analyzed in this study. The segmentations are shown in Table 3.

It was found in this study that the wave velocity subsection analysis was more complex than the variable coefficient subsection analysis. The microcrack comprehensive development stage included the microcrack stabilization development stage, as well as the microcrack accelerated development stage. The development of the microcracks was predominant during this stage. The microcrack–macrocrack transformation stage included the crack shift stage and the crack continued development stage. The

**Table 3** Segmentations of the different parameters

Wave velocity	Coefficient of variation	Porosity function–permeability model
Microcrack stabilization development stage ( $50 < T < 250$ °C)	Microcrack comprehensive development stage ( $50 < T < 300$ °C)	Stage 1 ( $50 < T < 200$ °C)
Microcrack accelerated development stage ( $250 < T < 300$ °C)		Stage 2 ( $200 < T < 400$ °C)
Crack shift stage ( $300 < T < 350$ °C)	Microcrack–macrocrack transformation stage ( $300 < T < 700$ °C)	
Crack continued development stage ( $350 < T < 700$ °C)		Stage 3 ( $400 < T < 700$ °C)

development of the macrocracks was predominant during this stage.

Stage 1 of the permeability model corresponded to most of the microcrack stabilization development stage. The geometrical factor and particle sizes did not change during this stage. Stage 2 of the permeability model corresponded to the over 200 °C part of the microcrack stabilization development stage, microcrack accelerated development stage, crack shift stage, as well as the under 400 °C part of crack continued development stage. The geometrical factor and particle sizes changed greatly during this stage which was apparent from the changes of the fitting curves slopes. Stage 3 of the permeability model corresponded to the over 400 °C part of crack continued development stage. The geometrical factor and particle sizes tended to be stable during this stage. The differences in the subsection bases of the different parameters led to differences in the subsection knots. Generally speaking, all of the analyses were dependent on the degree of crack development in the samples.

## 5 Conclusions

In this study, the granite wave velocity, wave velocity anisotropy and permeability following high-temperature processing at atmospheric pressure were measured. The conclusions which were reached were as follows:

1. The  $P$  and  $S$  wave velocities of the granite almost decreased linearly with the increasing temperatures. The wave velocity dropped significantly at 300 and 650 °C. In contrast to the wave velocity at 300 °C, the wave velocity at 350 °C showed only slight changes, as well as a possible reversing trend. Based on the wave velocity changing situation under the different temperatures, the thermal cracking could be divided into four stages as follows: the microcrack stabilization development stage, microcrack accelerated development stage, crack shift stage and crack continued development stage.
2. The coefficient of variable can be used to reflect the change in the structural feature of the cracks in the examination of wave velocity anisotropy. It was observed to increase with the increasing temperatures below 300 °C and remained almost unchanged with the temperatures above 300 °C. These findings suggested that the structures of the cracks had changed when temperatures were over 300 °C. The development of the microcracks was observed to be predominant under 300 °C, and the developments of the macrocracks was predominant over 300 °C.
3. The granite permeability increased almost exponentially with the increasing temperatures. It was found that above 350 °C, the growth rate of the permeability was speeded up. The permeability at 700 °C was confirmed to have increased by several hundred times that at the normal temperature and has changed slightly or even declined at 350 °C. These changes conformed to the wave velocity changes during this stage.
4. The porosity function  $f(\varphi) = \frac{\varphi^3}{(1-\varphi)^2}$  was used as the variable to analyze the relationship between  $f(\varphi)$  and permeability with following results: between 50 and 200 °C, the permeability was determined by the microcracks; 200–400 °C was considered to be a transition stage; and between 400 and 700 °C, the permeability was determined by the macrocracks. It was determined in this study that the fitting degrees of the three specimens were all high
5. The crack evolution for the Maluanshan granite after high-temperature processing is obtained after comparing the inversion results of the cracks with the wave velocity, wave velocity anisotropy and permeability.

Almost all of the heat treatments in the studies mentioned above regarding the effect of temperature on rock physical and mechanical properties were conducted at atmospheric pressure, thus differing from heat treatment performed under confining pressure. Wang et al. (1989) studied the change

rule of the AE properties of Westerly granite with temperature under different confining pressures (7, 28, 55 MPa), and observed that the initial temperature of AE events increased with increasing temperature, while the numbers of AE events decreased with the increasing temperature. Molen (1981) studied the change rule of the volumetric strain of quartz with temperature under different confining pressures (100, 200, 300 MPa) and concluded that the temperature–volumetric strain curve merely shifted with the increasing confining pressure, while the phase transition temperature of quartz increased with the increasing temperature. Somerton et al. (1965) found that compared with atmospheric pressure the physical properties (such as sound velocity, permeability and fracture index) of sandstone changed slightly with temperature under 1500 psi (10 MPa) confining pressure. In a study of the change rule of the linear thermal expansion coefficient of Climax quartz monzonite with temperature under different confining pressures (0, 13.8, 27.6 MPa), Heard (1980) also observed a similar law.

The in situ stress of the Maluanshan granite in this study was only 5 MPa. Although the specimens were heated at atmospheric pressure, the wave velocities and permeability were measured under 5 MPa confining pressure. Therefore, the experimental results should be closer to the values which were heated under 5 MPa confining pressure. Heat treatment under confining pressure will cause some differences in the properties of rock. This is because, when the rock is heat-treated under confining pressure, some thermal stresses can be counteracted, and the number of heat cracks will decrease. Therefore, in future research, the effect of confining pressure on heat treatment results should be studied in detail.

**Acknowledgements** This study was financially supported by the National Natural Science Foundation of China (51622404, 51374215 and 11572343), the State Key Research Development Program of China (2016YFC0801404) and Outstanding Young Talents of “Ten Thousand People Plan.” Additionally, we would like to thank Prof. Ye from California State University and Dr. Yu from Columbia University, who provided Language Guide for the paper.

## References

- Bauer SJ, Johnson B (1979) Effects of slow uniform heating on the physical properties of the Westerly and Charcoal granites. In: 20th US symposium on rock mechanics (USRMS). American Rock Mechanics Association
- Benson P, Schubnel A, Vinciguerra S, Trovato C, Meredith P, Young RP (2006a) Modeling the permeability evolution of microcracked rocks from elastic wave velocity inversion at elevated isostatic pressure. *J Geophys Res Solid Earth* 111:B04202
- Benson PM, Meredith PG, Schubnel A (2006b) Role of void space geometry in permeability evolution in crustal rocks at elevated pressure. *J Geophys Res Solid Earth* 111:B12203
- Carman PC, Machefer J (1961) L'écoulement des gaz a travers les milieux poreux. Institut National Des Sciences Et Techniques Nucleaires Presses Universitaires De France, Paris
- Casse FJ, Ramey HJ Jr (1979) The effect of temperature and confining pressure on single-phase flow in consolidated rocks (includes associated paper 9087). *J Pet Technol* 31:1051–1059
- Chaki S, Takarli M, Agbodjan WP (2008) Influence of thermal damage on physical properties of a granite rock: porosity, permeability and ultrasonic wave evolutions. *Constr Build Mater* 22(7):1456–1461
- Chen Y, Wu X, Zhang F (1999) Experiments on thermal fracture in rocks. *Chin Sci Bull* 44(17):1610–1612 (in Chinese)
- Chen Y, Kobayashi T, Kuriki Y, Kusuda H, Mabuchi M (2008) Observation of microstructures in granite samples subjected to one cycle of heating and cooling. *J Jpn Soc Eng Geol* 49(4):217–226
- Chen S, Yang C, Wang G (2017) Evolution of thermal damage and permeability of Beishan granite. *Appl Therm Eng* 110:1533–1542
- Dang J, Zhou Y, Rybacki E, He C, Dresen G (2016) An experimental study on the brittle–plastic transition during deformation of granite. *J Asian Earth Sci* 139:30–39
- Fredrich JT, Wong Tf (1986) Micromechanics of thermally induced cracking in three crustal rocks. *J Geophys Res Solid Earth* 91:12743–12764
- Freire-Lista D, Fort R (2017) Exfoliation microcracks in building granite. Implications for anisotropy. *Eng Geol* 220:85–93
- Freire-Lista DM, Fort R, Varas-Muriel MJ (2016) Thermal stress-induced microcracking in building granite. *Eng Geol* 206:83–93
- Heard HC (1980) Thermal expansion and inferred permeability of climax quartz monzonite to 300 °C and 27.6 MPa. *Int J Rock Mech Min Sci Geomech Abstr* 17(5):289–296
- Homand-Etienne F, Houpert R (1989) Thermally induced microcracking in granites: characterization and analysis. *Int J Rock Mech Min Sci Geomech Abstr* 26(2):125–134
- Inserra C, Biwa S, Chen Y (2013) Influence of thermal damage on linear and nonlinear acoustic properties of granite. *Int J Rock Mech Min Sci* 62:96–104
- Jones C, Keaney G, Meredith PG, Murrell SAF (1997) Acoustic emission and fluid permeability measurements on thermally cracked rocks. *Phys Chem Earth* 22:13–17
- Lin W (2002) Permanent strain of thermal expansion and thermally induced microcracking in Inada granite. *J Geophys Res Solid Earth* 107(B10):2215
- Molen IVD (1981) The shift of the  $\alpha$ – $\beta$  transition temperature of quartz associated with the thermal expansion of granite at high pressure. *Tectonophysics* 73(4):323–342
- Morrow C, Lockner D, Moore D, Byerlee J (1981) Permeability of granite in a temperature gradient. *J Geophys Res Solid Earth* 86:3002–3008
- Nara Y, Kaneko K (2007) Properties of P-wave propagation in granite with changes in temperature and humidity. *J Soc Mater Sci Jpn* 56:803–808
- Raymer LL, Hunt ER, Gardner JS (1980) An improved sonic transit time-to-porosity transform. In: SPWLA 21st annual logging symposium. Society of Petrophysicists and Well-Log Analysts
- Richter D, Simmons G (1974) Thermal expansion behavior of igneous rocks. *Int J Rock Mech Min Sci Geomech Abstr* 11:403–411
- Simmons G, Cooper HW (1978) Thermal cycling cracks in three igneous rocks. *Int J Rock Mech Min Sci Geomech Abstr* 15:145–148
- Somerton WH, Mehta MM, Dean GW (1965) Thermal alteration of sandstones. *J Pet Technol* 17(5):589–593
- Takarli M, Prince-Agbodjan W (2008) Temperature effects on physical properties and mechanical behavior of granite: experimental investigation of material damage. *J ASTM Int* 5:1–13
- Wang HF, Bonner BP, Carlson SR, Kowallis BJ, Heard HC (1989) Thermal stress cracking in granite. *J Geophys Res Solid Earth* 94(B2):1745–1758

- Weinbrandt RM, Ramey HJ Jr, Casse FJ (1975) The effect of temperature on relative and absolute permeability of sandstones. *Soc Pet Eng J* 15(05):376–384
- Xi DY (1994) Physical characteristics of mineral phase change in granite. *Acta Mineralogica Sinica* 03:223–227 **(in Chinese)**
- Yong C, Wang C (1980) Thermally induced acoustic emission in Westerly granite. *Geophys Res Lett* 7(12):1089–1092
- Zhang W, Sun Q, Hao S, Geng J, Lv C (2016) Experimental study on the variation of physical and mechanical properties of rock after high temperature treatment. *Appl Therm Eng* 98:1297–1304
- Zhao Y, Wan Z, Feng Z, Yang D, Zhang Y, Qu F (2012) Triaxial compression system for rock testing under high temperature and high pressure. *Int J Rock Mech Min Sci* 52:132–138
- Zuo JP, Xie HP, Zhou HW, Peng SP (2007) Experimental research on thermal cracking of sandstone under different temperature. *Chin J Geophys* 50(4):1150–1155 **(in Chinese)**
- Zuo JP, Zhou HW, Fang Y, Meng BB, Peng RD (2011) Experimental research on thermal cracking of deep granite in Beishan region, Gansu Province. *Chin J Rock Mecha Eng* 06:1107–1115 **(in Chinese)**